Nanocarbon-based catalysts for esterification: effect of carbon dimensionality and synergistic effect of the surface functional groups

Honglei Zhang [a], Xiang Luo [b], Kaiqi Shi [b], Tao Wu [b, c], Feng He [d], Hangqi Yang [a], Shanshan Zhang [a], Chuang Peng [a,*]

[a] School of Resource and Environmental Sciences, Hubei International Scientific and Technological Cooperation Base of Sustainable Resource and Energy, Wuhan University, Wuhan, 430072, P. R. China.

[b] New Materials Institute, The University of Nottingham Ningbo China, Ningbo, 315100, P.R. China.

[c] Municipal Key Laboratory of Clean Energy Conversion Technologies, The University of Nottingham Ningbo China, Ningbo, 315100, P.R. China.

[d] College of Environment, Zhejiang University of Technology, Hangzhou Zhejiang, 310014, China.

Abstract

Carbon-based solid acid catalysts represented outstanding hydrothermal and mechanical properties but lower catalytic performances and stabilities. Therefore, more comprehensive investigations should be conducted to optimize their catalytic performances. The correlations between catalytic performance, carbon dimensionality and composition of oxygen-containing functional groups of nanocarbon-based catalysts were investigated. The dimensionality of carbon materials had notable effect on the catalytic reactivity and the layered 2-D structure could maximize the solid/liquid interface and minimize the mass transfer resistance and thus favor the catalytic esterification. GO-50, prepared with 50 mL concentrated H_2SO_4, exhibited outstanding catalytic activity and had 3 times higher turnover frequency (TOF) value than that of H_2SO_4. In GO-50, the $-SO_3H$ groups were identified as the primary catalytic active sites, while the carboxyl groups enhanced the inherent activity of $-SO_3H$, thus facilitating the esterification. The $-COOH/-SO_3H$ molar ratio played significant roles and desirable $-COOH/-SO_3H$ molar ratio would promote esterification significantly. The esterification kinetics catalyzed by GO-50 was studied and the apparent activation energy of esterification by GO-50 is 1.5 times lower than that by H_2SO_4. The esterification mechanism by GO-50 was also proposed. Furthermore, GO-50/Poly (ether sulfones) (PES) membrane was prepared and employed in esterification and the optimal reaction conditions were systematically studied.

Keywords: Catalytic activity; Carbon-based solid acid catalyst; Esterification; Graphene oxide; Reaction kinetics

1. Introduction

Due to the awareness of the depletion of the world's limited energy reserves and the increasing environmental concerns, there is an increasing demand for green and renewable energy sources over the past years [1]. Biodiesel, which can be blended with petroleum-based diesel fuels and be used directly in current engines, is

considered a promising substitute for fossil fuels as it is biodegradable, renewable, easy to store, inherently safe and non-toxic [2]. Biodiesel can be produced from the esterification or transesterification of renewable sources (vegetable oils or animal fats) with alcohols in the presence of an acidic or alkaline catalyst [3]. Commercial biodiesel, i.e., methyl ester, is produced via esterification of free fatty acids (FFAs) with methanol and the transesterification of triglyceride with methanol.

Despite the advantages mentioned above, biodiesel has not currently become competitive compared to fossil fuels due to its higher cost of raw material and production. One way to reduce the cost of biodiesel is to use cheaper oil feedstock like waste cooking oils (WCO) [4, 5]. The main disadvantage of using WCO as the raw material is that WCO contains a large amount of free fatty acids (FFAs) which normally react with the alkaline catalyst to form soap [6]. Therefore, the high free fatty acid contents in WCO have to be pre-esterified with methanol under the presence of homogeneous acid catalysts, such as sulfuric acid and hydrochloric acid [7, 8]. Homogeneous catalysis reaction is the most commonly used commercial process for the manufacture of a wide range of important chemicals such as pharmaceuticals and petrochemicals. However, there are still several intrinsic drawbacks of using homogenous catalysts, such as difficulty of separating the catalyst from the reaction mixtures, poor stability of the catalysts, formation of large amount of wastewater and corrosion of apparatus [8]. In contrast, heterogeneous catalysis offer the advantages of easier separation, longer catalyst life, lower corrosion and more efficient recycling, thus reducing the overall production costs [9]. Versatile solid acid catalysts have been investigated spanning cation-ion-exchange resins [10], sulphated and tungstated zirconia [11, 12], silica-based catalysts , zeolites [13], catalytic membranes [6, 14, 15], and carbon-based solid acid catalysts [2, 16-19].

With the merits of being metal-free, stable and recyclable, various carbon-based solid acid catalysts such as sulfonated activated carbon, sulfonated aromatic compounds, sulfonated hydrothermal carbon (S-HTC), glucose-p-toluene sulfonic acid (Glu-TSOH), sugar catalyst, S-SWCNTs, S-MWCNTs, cellulose-derived carbon solid acids (CCSAs), functional-MWCNTS, HPA-doped activated carbon fibers,

hydrothermally sulfonated single-walled carbon nanohorns, sulfonated ordered mesoporous carbon and sulfonated reduced graphene oxide (S-RGO) have been synthesized and applied in acid-catalyzed reactions [2, 9, 18, 20-28]. Despite excellent catalytic activities, the preparations of these above catalysts always need too much concentrated sulfuric acid and complicated process. Among all the carbon materials, graphene has attracted much research interest owing to its excellent thermal and mechanical stability, extraordinary electrical conductivity, high surface area and ultra-high degree of exposure of active sites, endowing it a promising catalyst carrier with ultra-high accessibility of catalytic active sites [29-33]. The most commonly used scalable approach for preparation of graphene involves graphite oxidation to form GO and reduction to yield reduced graphene oxide (RGO or graphene) [25, 34-36]. Although the accurate structure is difficult to determine, GO is a nonconductive hydrophilic carbon material with abundant hydrophilic functional groups including hydroxyl, carboxyl, and epoxy groups (Fig.S1) [37-39]. These oxygen-containing functional groups can lead to mild acidic and water adsorbing properties. Besides, during the preparation process of GO using Hummer's method, a small quantity of $-SO_3H$ groups was inserted in the GO, which endows GO with unusual feature of strong Brønsted acid [40-42]. Thus, GO have been demonstrated to be an effective green solid acid catalyst for selective hydrolysis of cellulose to glucose and for the production of alkyl levulinates by alcoholysis [40, 42].

Despite the fact that these carbon-based solid acid catalysts represented outstanding hydrothermal and mechanical stability, they encountered lower catalytic performances and leaching problem which limited their application, especially in the continuous catalysis. In addition, the effects of the composition of oxygen-containing functional groups and carbon dimensionality of nanocarbon on the catalytic performance have not been studied. In this work, a holistic study is conducted to establish the above correlations in esterification of oleic acid with methanol using nanocarbon catalysts. The best performing catalyst is identified and a synergistic effect is found between the $-SO_3H$ and $-COOH$ groups. The reaction kinetics and mechanism of esterification of this catalyst is discussed in detail. Additionally,

GO-50/PES composite membrane was prepared and the catalytic performance was also examined by the same esterification reaction.

2. Experiment details

2.1 Materials

Graphite powder (300 mesh) with a purity of 99.9% was purchased from Aladdin (Shanghai, China). Single walled and multiple walled carbon nanotubes (SWCNTs and MWCNTs) were supplied by Chengdu Organic Chemicals CO., LTD. CAS (China). Amberlyst-15 purchased from Acros Organics (USA) was milled in frozen state using liquid nitrogen to obtain fragments (~24.96 μm) and used as a control. PES was purchased from Solvay Advanced Polymer Co. Ltd. H_2SO_4, $KMnO_4$, oleic acid and other chemicals in AR grade were commercially purchased from Sinopharm Chemical Reagent Co., (SCRC, China) and used without further purification.

2.2 Preparation of GO samples

2.2.1 Preparation of FGO (GO-50, GO-75 and GO-100)

Functional graphene oxide (FGO) samples were prepared by a modified Hummers' method. Varied contents of functional groups were obtained by controlling the amount of concentrated sulfuric acid. Briefly, 3.0 g of graphite powder and 1.5 g of sodium nitrate ($NaNO_3$) were mixed with certain volume (50, 75 and 100 mL, respectively) of concentrated sulfuric acid in an ice bath, while maintaining agitation. The volume of sulfuric acid is larger than 50 mL in this work because less volume would lead to thick solution, making it difficult to preparation FGO. Then 9.0 g of potassium permanganate ($KMnO_4$) powders were slowly added into the suspension while keeping the reaction temperature below 20 ℃ for 7 h. Additional 9.0 g of $KMnO_4$ was added in one portion, and the reaction was stirred for 12 h at 35 ℃. The reaction mixture was cooled to room temperature and poured onto ice (~400 mL) with 30 % H_2O_2 (3 mL). The suspension was centrifuged till neutral pH and the supernatant was decanted away. The remaining solid was then washed in succession with 200 mL of 30 % HCl, 200 mL of ethanol, and 200 mL of boiling DI water till neutral pH. The material remaining was coagulated with 200 mL of ether, and the

resulting suspension was filtered, and vacuum-dried overnight at room temperature to obtain brown-colored graphite oxide (GOite). After that, aqueous suspension of the graphite oxide was undertaken sonication for 1 h and vacuum-dried to obtain the final FGO (denoted as GO-50, GO-75 and GO-100 according to the volume of sulfuric acid used).

2.2.2 Preparation of GO-2

GO-2 was obtained by using traditional Hummers' method [43]. 10 g of graphite powder and 5 g of sodium nitrate was added to 230 mL of concentrated sulfuric acid with stirring in an ice-bath. After agitation for 1 h, 30 g of potassium permanganate was added slowly into the suspension, during which the temperature was kept under 20 ℃. Then, the ice-bath was removed and the temperature of the suspension was increased to 35 ℃ and maintained for 0.5 h. 500 mL of water was slowly added into the paste under vigorous stirring, and the temperature was raised to 98 ℃ and maintained for 15 minutes. The suspension was then further diluted into 1 L of warm water and treated with 37 mL of hydrogen peroxide. The suspension was vacuum filtered to obtain a brown filter cake that was washed for five times with 1 L of warm water till neutral pH to yield graphite oxide suspension. The aqueous suspension was sonicated for 1 h, centrifuged and vacuum-dried at room temperature for 24 hours to obtain 14 g of GO-2.

2.2.3 Preparation of GO-3

GO-3 was prepared by a modified Hummers' method [37]. Briefly, 3 g of graphite powder and 18 g of $KMnO_4$ were added into a mixture of concentrated H_2SO_4/H_3PO_4 (360/40 mL) and maintained at the temperature between 35-40 ℃. The reaction suspension was then heated to 50 ℃, stirred for 12 h and then cooled to room temperature and poured into 400 mL ice with 3 mL of 30 % H_2O_2. The mixture was vacuum filtered and the filtrate was centrifuged till neutral pH, and the supernatant was decanted away. The remaining solid material was then washed 2 times in succession with 30 % HCl, ethanol, and boiling water till neutral pH. The solid obtained on the filter was vacuum-dried overnight at room temperature, obtaining 4 g of GO-3.

2.2.4 Preparation of S-GO-50

The as-prepared GO-50 was sulfonated with concentrated sulfuric acid at 200 ℃ for 24 h to produce sulfonated-GO-50 (denoted as S-GO-50). Briefly, 1 g of GO-50 was dissolved in 50 mL of sulfuric acid and stirred for 5 hours till a homogeneous aqueous suspension was obtained. Then the aqueous suspension was transferred into a PTFE autoclave with 80 mL capacity, was heated to 200 ℃ for 4 hours. Then, the suspension was cooled naturally to 25 ℃. The black precipitate was collected by filtration, followed by sequential washing with 30 % HCl, ethanol, and boiling DI water till neutral pH. The black samples were then dried in vacuum at 60 ℃ for 24 hours to obtain 1.1 g of S-GO-50. Abbreviations for all the FGO samples used in this work are illustrated in Table 1.

Table 1 Abbreviations for all the FGO samples

Abbreviation	Sulfuric acid volume (mL)	Reference
GO-50	50	This work
GO-75	75	This work
GO-100	100	This work
GO-2	69	[43]
GO-3	360	[37]
GOite-50	50	This work
S-GO-50	50	This work

2.3 Preparation of GO-50/PES composite membrane

20 g of poly (ether sulfone) (PES) was dissolved in 80 g of NMP under continuous stirring at room temperature for 12 hours to obtain homogeneous suspension. Then 4 g of GO-50 was added into the above suspension and stirred for another 24 hours. The suspension was cast onto a glass plate and copper wires with outer diameter of 0.1, 0.2 and 0.5 mm were used to control the membrane thickness, respectively. The glass plate was immersed into deionized water to phase inversion and then the membranes were peeled off from the glass plate and allowed to dry in a

vacuum oven at 50 ℃ for 24 hour to remove the trace water. The solid membranes obtained were then annealed at 150 ℃ for 1 h in a heating oven. Finally, the GO-50/PES membranes were cut into small pieces (0.5 cm $\times$ 0.5 cm) for further use.

2.4 Catalyst characterization

2.4.1 Surface morphology and phase structures of the catalysts

The surface morphology of all the solid acid catalysts prepared was inspected under a Zeiss Ultra Plus Field-Emission Scanning Electron Microscope (FESEM) (Zeiss Co., Germany) equipped with an energy dispersive X-ray (EDX) detector. A TEM measurement was carried out on a JEOL JEM 2100 UHR transmission electron microscope operated at 200 kV. The phase structures of powders were studied using the powder X-ray-diffraction (XRD, Bruker D8 Advance) technique. The measurement was proceeded with Cu K_α radiation (λ = 0.1542 nm) at a step of 0.02 °/s in the Bragg angle (2 theta) range from 5 ° to 60 °.

2.4.2 Spectral analysis

The IR spectra of the prepared GO samples were characterized by Fourier Transform Infrared Spectroscopy (FTIR) TENSOR-37 (Bruker Co.) operated by Attenuated Total Reflectance (ATR) in the wavenumber range of 4000-500 cm^{-1}. Raman spectra in the range of 1000-2200 cm^{-1} were acquired by an inVia-reflex (Renishaw co., UK) confocal microscopy Raman spectrometer using a laser excitation wavenumber of 532 nm with a resolution of 1 cm^{-1}. Ultraviolet-Visible (UV-Vis) diffuse reflectance spectra of all the samples were recorded by Evolution 201 (Thermal Scientific Co.) equipment at room temperature in the range of 190-800 cm^{-1}. X-ray photoelectron spectroscopy (XPS) analyses of the samples were carried out on a Kratos AXIS Ultra DLD photoelectron spectrometry (Kratos Analytical Ltd., UK) using monochromatic Al-Kα radiation source at 1486.6 eV. High-Resolution X-ray photoelectron spectroscopy (HRXPS) spectra of O 1s and S 2p were an average of 4 scans acquired at pass energy of 10 eV and a resolution of 0.05 eV per step.

2.4.3 Elemental, Acid densities and strength analysis

The percentages of carbon (C), hydrogen (H), nitrogen (N), and sulfur (S) of the samples were determined by using a 2400 Series II CHNS/O Elemental Analyzer

(Perkin Elmer, USA). The oxygen (O) content was calculated by the difference. The compositions of all the samples were also characterized using an energy dispersive X-ray spectroscopy (EDX) (Oxford, UK) attached to the SEM. Acid-base titration with NaOH (0.05 M) was used to obtain total acidity while sulfur elemental analysis used to calculate the -SO_3H density in catalysts. In addition, Boehm titration method was used to obtain the acid density of -COOH groups [44, 45]. Besides, the pH of each carbon-based solid catalyst (300 mg) was measured in DI water (27 mL) after stirring for 1 h under N_2 atmosphere. The pH of sulfuric acid (3.8 mmol L^{-1}) and acetic acid (3.8 mmol L^{-1}) was also measured as control. The reported values were the means of at least five measurements and the average experimental error was ±5 %.

2.4.4 Thermal stability

Thermal properties of the catalysts were determined by a STA449F3 Jupiter Thermo-gravimetric Analyzer (TGA, Netzsch Co., Germany). Differential Scanning Calorimeter (DSC) measurements were carried out concurrently in the same range of 105 to 900 ℃.

2.5 Esterification catalyzed by different catalysts

Esterification reactions were performed in a three-necked batch reactor (250 mL) equipped with a reflux condenser and a mechanical stirrer at atmospheric pressure. The oleic acid was first introduced into the reactor and heated to the desired temperature. Then the desired amount of the methanol and the catalyst were added into the reactor and the reaction began at pre-determined conditions. The primary reaction conditions were as follows: oleic acid, 20 g; methanol/oleic acid molar ratio 30: 1; catalyst loading 0.1 g; mechanical stirring, rate 360 rpm; reaction temperature, 338 K; and reaction time, 8 h, except otherwise mentioned. The samples were taken out from the reactor every hour and the composition was tested on a Gas Chromatography (GC 7890B, Agilent Technologies) with a flame ionization detector equipped with a HP-5 column to get oleic acid conversion and esterification yield. After completion, the reaction mixture was poured into a separating funnel and allowed to settle for 1 h to separate the excess methanol and the biodiesel.

2.6 Recycle test

After each run, the solid catalysts were separated by centrifugation from the reaction mixture and dispersed in deionized water. Then the samples were first washed with ethyl ether twice to remove the adsorbed organic components and then washed with ethanol, boiling DI water twice, respectively. Afterward, the sample dispersed in deionized water was sonicated for another 30 min. The recovered catalysts were then dried in a vacuum oven at 50 ℃ for 24 h to remove residual water completely prior to being reused in the recycling tests.

3. Results and discussion

3.1 Characterization of GO samples

3.1.1 Surface morphology of pristine graphite powder, GO-50 and S-GO-50

The morphology of pristine graphite powder, GO-50 and S-GO-50 were studied by using SEM and TEM. As shown in Fig. 1(a), graphite particles are in the bulky crystalline form of carbon and show micro-scale (300 mesh, <50 μm) irregular particle grains. After harsh oxidation and ultra-sonication treatment, GO-50 sheets became smaller and transparent and some thin flakes can be found due to the decrease of Van der Waals interactions between the graphite layers caused by the introduction of oxygen-containing functional groups (Fig. 1 (b)) [46]. SEM of S-GO-50 in Fig. 1(c) shows almost the same microstructure with that of GO-50, suggesting that the sulfonation treatment does not affect the microstructure of GO-50. TEM image in Fig. 1(d) also demonstrates that the GO-50 has transparent lamella and irregular wrinkled edges, indicating mono- or few-layer planar sheet structure of GO-50 [46]. In addition, SEM and TEM pictures of several typical carbon-based solid acidic catalysts were also illustrated in Fig. S13.
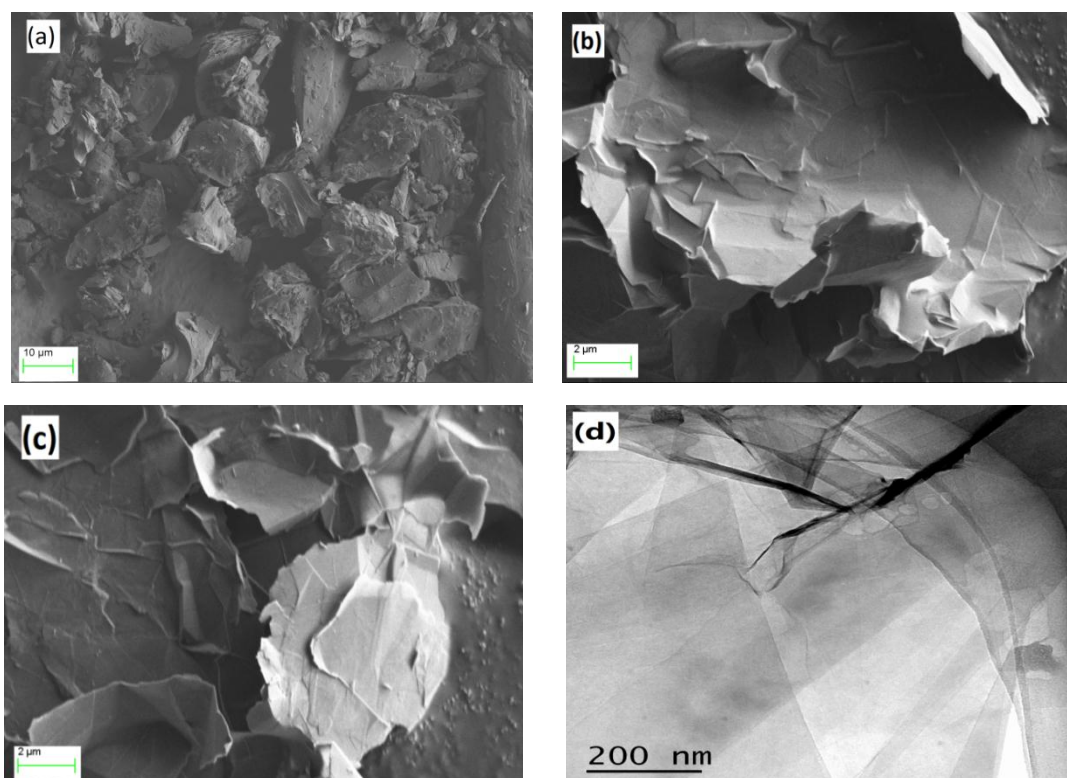
Fig.1 Representative SEM of graphite (a), GO-50 (b), S-GO-50 (c) and TEM (d) of

GO-50

3.1.2 XRD of FGO samples

The phase structures of graphite and all the the FGO samples were characterized by XRD measurements and the results are illustrated in Fig. 2. The prisite graphite shows a typical diffraction peak (002) of graphite (2θ=26.5 °, corresponding to d-spacing of 0.34 nm). However, the (002) peak disappears completely in all the FGO samples, suggeating that the prisite graphite has been successfully oxidized to GO [47, 48]. The XRD patterns of all the FGO samples show new diffraction peaks at approximately 2θ=11 ° with significant decreases in graphite crystallinity due to a lattice expansion after harsh oxidation treatment [48, 49]. In addition, the d-spacing increases from 0.72 nm to 0.84 nm when the sulfuric acid usage increases from 50 to 100 mL, suggesting that more oxygen-containing functional groups were inserted into the graphite layers [45].
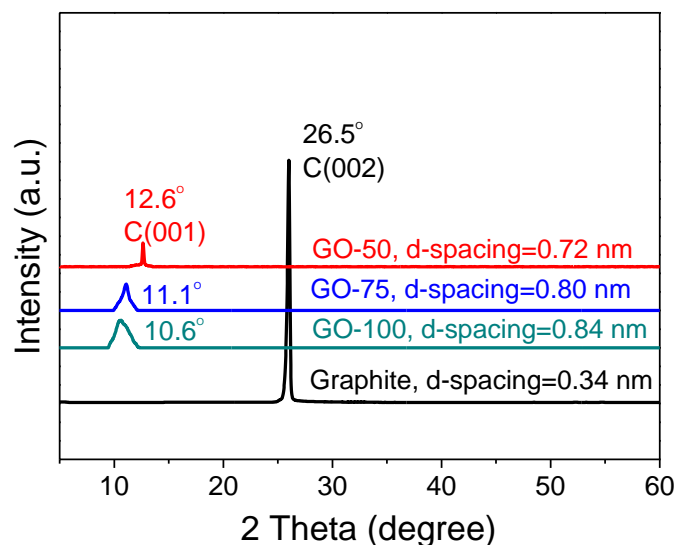
Fig.2 XRD patterns of graphite, GO-50, GO-75, and GO-100

3.1.3 Spectral analysis of FGO samples

The FTIR spectra of graphite and all the FGO samples are shown in Fig. 3. The pristine graphite exhibits no adsorption peaks in the finger print region because it is free of oxygen-containing functional groups. However, FTIR curves of all the FGO samples show various adsorption peaks in the range of 1000-1750 cm^{-1}. GO-50, GO-75 and GO-100 possess several characteristic adsorption peaks, confirming the presence of abundant oxygen-containing functional groups and the successful synthesis of FGO. Specifically, the two obvious peaks at 1710 cm^{-1} and 1620 cm^{-1} indicates the C=O stretching vibration form -COOH and the aromatic C=C skeletal vibrations from un-oxidized graphitic domains, respectively [50]; the two strong peaks at 1400 and 3440 cm^{-1} represent the deformation vibration and the stretching vibration of O-H; the peaks at 1000 and 1030 cm^{-1} were assigned to the symmetric O=S=O stretching vibrations and S-C stretching vibration from -SO_3H groups [51]; the peak at 1240 cm^{-1} was caused by C-O-C groups from the epoxides groups. In addition, all these peaks become stronger with the increase of sulfuric acid usage due to higher degree of oxidation, which is in consistence with the XRD results (Fig. 2). Compared with the FTIR curve of GO-50, S-GO-50 possesses weaker peaks in 1710 cm^{-1} and 1620 cm^{-1}, while much stronger peaks in 1000 and 1030 cm^{-1}, suggesting that the -COOH and C=C groups have been mostly sulfonated into -SO_3H groups
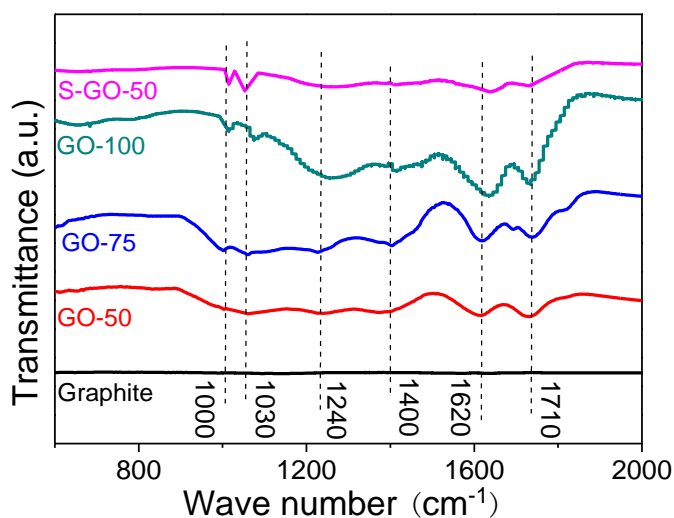
after H_2SO_4 treatment.

Fig.3 FTIR spectra of graphite and all the FGO samples

Raman spectroscopy is a powerful nondestructive tool to characterize carbonaceous materials, particularly for ordered and disordered crystal structures of carbon. Usually, the D/G band intensity ratio (I_D/I_G) could be used to evaluate the structural changes during the chemical processing. Raman spectra in the range of 1000-2200 cm^{-1} were used to characterize the structural changes occurring during the oxidation treatment (Fig. 4). The pristine graphite shows a prominent G band at 1574 cm^{-1}, corresponding to vibration of sp^2 carbon atoms in a graphitic two-dimensional (2D) hexagonal lattice and a weak D band at 1348 cm^{-1} associated with the vibration of sp^3 carbon atoms of defects and disorder [52, 53]. The I_D/I_G of graphite is calculated to be approximately 0.2 due to the large grain size of pristine graphite and little disorder (as shown in Fig. 1 (a)) [48]. However, in the Raman spectrum of FGO samples, the G bands for all the FGO samples become wide and shifted to 1583 cm^{-1}, suggesting increased oxidation degree and more oxygen-containing functional groups were grafted on the FGO surface [52]. In addition, the D band at 1348 cm^{-1} becomes prominent due to and reduction of the in-plane sp^2 domains after the harsh oxidation. Furthermore, the I_D/I_G values increase from 0.82 to 1.14 with increasing sulfuric acid dosage, indicating more structural disorder caused by more oxygen-containing functional groups, which agree well with the XRD and FTIR results illustrated in Fig. 2 and Fig. 3. It is also noted that GO-50 and S-GO-50 possess almost the same I_D/I_G,

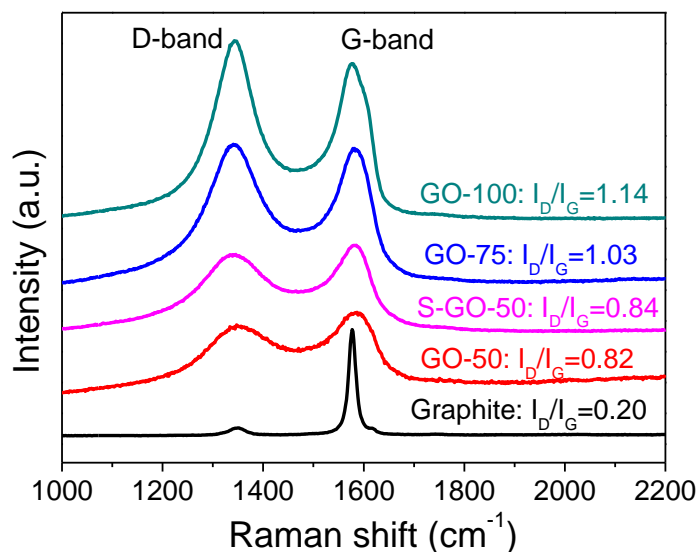suggesting that the sulfonation treatment does not affect the structure integrity of GO-50.

Fig.4 Raman spectra of graphite, GO-50, GO-75, GO-100 and S-GO-50

Ultraviolet-visible (UV-Vis) absorption spectroscopy was also employed to understand the dispersion stability of GO in aqueous suspension. Fig. 5 shows the UV–Vis curves of supernatants of the graphite and the three FGO suspensions (0.2 mg mL^{-1}) which had undergone sonication and settlement for 2 weeks. No absorption peaks were found for graphite suspension in the measured scale, indicating that almost all of the graphite precipitated after 2 weeks and graphite dispersion in water was not stable. However, the spectra of all the FGO samples exhibited two characteristic absorption features that could be used as a means of identification. The strong absorption band at 230 nm is correspond to $\pi\rightarrow\pi^*$ transitions of C=C double bond and the weak shoulder at around 300 nm is assigned to $n\rightarrow\pi^*$ transitions of C=O bond [54]. The two peaks further confirmed the successful synthesis of FGO. The digital photographs of graphite and FGO suspensions with concentration of 0.2 mg mL^{-1} are illustrated in Fig.S2. Graphite suspension was well dispersed after sonication but completed precipitate was observed after 2 weeks, indicating short-term stability. However, all the three FGO samples formed brown and stable dispersions even after 2 weeks due to the presence of hydrophilic oxygen-containing functional groups on FGO [54]. Both the UV-Vis results (Fig. 5) and the visual

inspection indicated that the prepared FGO samples exhibited long-term stability in water, which would facilitate their manipulation and processing for different applications [55].
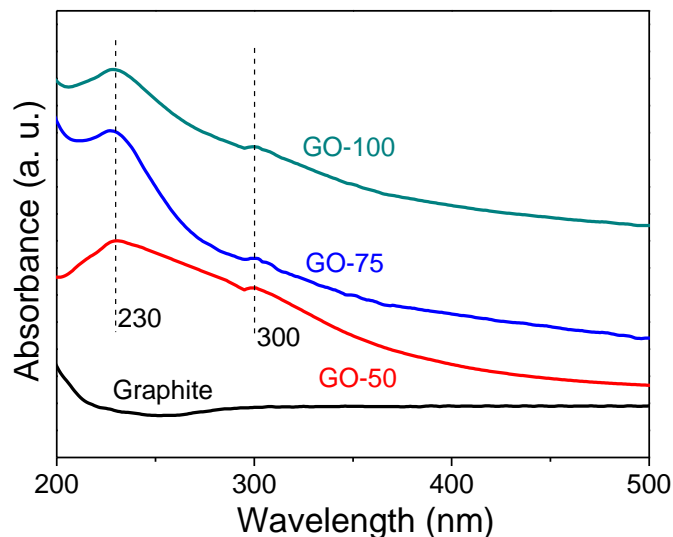

Fig.5 UV-Vis spectra of supernatants of graphite and FGO samples

(Concentration=0.2 mg mL^{-1})

3.1.4 Elemental, acid density and strength analysis

The data derived from elemental analysis, acid-base titration and Boehm titration is shown in Table 2. The pristine graphite contains only trace amount of O content and no sulfur content while all the FGO samples possess both S and O elements after oxidation. It is noted that S content, O content, total acidity, -SO$_3$H density and S/C mass ratio increased with the increase of sulfuric acid usage for GO-50, GO-75 and GO-100, which is in consistent with the results of XRD (Fig. 2), FTIR (Fig. 3) and Raman analysis (Fig. 4). It is also noted that the total acidity value is higher than that of -SO$_3$H density for each individual sample, suggesting the presence of weak acidic groups such as -COOH groups. Compared with GO-50, S-GO-50 possess two times higher sulfur content, -SO$_3$H density and almost the same total acidity value, indicating that most of the weak acidic groups in GO-50 were transferred into -SO$_3$H groups after the sulfonation treatment. GO-2 and GO-3 possess less sulfur content and total acidity values compared with GO-50, GO-75 and GO-100 due to the excessive KMnO$_4$ usage in the preparation of the latter three samples [50]. The pH of the carbon

catalysts (300 mg) suspended in 27 mL of deionized (DI) water as well as 3.8 mmol L^{-1} sulfuric acid, acetic acid and oleic acid are also illustrated in Table 2. Sulfuric acid displays the lowest pH among all the catalysts due to its strong acid nature. The suspension of GO-50, GO-75 and GO-100 displayed higher pH than S-GO-50, sulfuric acid, acetic acid and Amberlyst-15; but lower than that of graphite, GO-2, GO-3 and oleic acid. Furthermore, the chemical compositions of GO-50, GO-75 and GO-100 obtained from elemental analysis are also illustrated in Fig.S3.

Table 2 Chemical and textural characteristics of graphite, FGO samples and several typical acidic catalysts

Samples	Element (wt. %) [a]			Total acidity (mmol g^{-1})[b]	-SO$_3$H density (mmol g^{-1})[a]	-COOH density (mmol g^{-1})[c]	S/C mass ratio (%) [a]	pH [d]
	C	S	O					
Graphite	98.7	0.0	1.0	-	-	-	-	6.8
GO-50	65.2	2.9	29.5	2.58	0.90	1.62	4.4	4.6
GO-75	60.7	3.4	31.8	3.53	1.06	2.27	5.6	4.5
GO-100	52.9	4.2	37.9	4.33	1.31	2.71	7.9	4.5
S-GO-50	64.9	6.7	26.8	2.56	2.09	0.32	10.4	4.2
GO-2	76.4	0.6	21.8	0.21	0.18	0.03	0.1	5.7
GO-3	73.5	0.8	24.4	0.32	0.27	0.05	0.1	5.0
Amberlyst-15	58.2	14.7	22.2	4.7	4.7	0	25.3	3.4
H$_2$SO$_4$	-	-	-	20.4	-	-	-	2.2
Acetic acid	-	-	-	-	-	16.7 [e]	-	3.7
Oleic acid	-	-	-	-	-	3.54 [e]	-	4.8

[a] obtained by elemental analysis; [b] determined by acid-base titration; [c] obtained by Boehm titration; [d] measured with a pH electrode (0.01 g mL^{-1} for solid catalysts, 3.8 mmol L^{-1} for liquid catalysts); [e] calculated by relative molecular weight.

The chemical states of GO-50 were further studied by XPS survey,

high-resolution C 1s and S 2p XPS spectra and the results are illustrated in Fig. 6. In brief, the C 1s XPS spectrum of GO-50 in Fig.6(a) shows one large broad peak with a collection of four smaller peaks related to sp^3 carbon (C-C bonds), epoxy (C-O-C bonds), carbonyl (C=O bonds), and carboxylate (O-C=O bonds) appearing at 284.6, 286.9, 287.9 and 289.3 eV, respectively [56]. It is also found that the peaks at 286.9 and 287.9 eV are higher than that of 284.6 eV, suggesting that oxygen-containing functional groups are dominant on GO-50 [57, 58]. The S 2p XPS spectrum of GO-50 in Fig. 6 (b) shows a single Gaussian distribution peak at 168.4 eV, which is assigned to the anticipated values for sulfonic acid groups [50]. In addition, the mass ratio of S to C of GO-50 derived from the peak area of the S 2p spectra is 4.52 %, while the value obtained by elemental analysis (Table 2) and EDX (Fig. S4) are 4.44 % and 4.58 %, respectively. Since EDX and XPS only scans the elements content at the surface (with scan depth lower than 10 nm) while elemental analysis examines the entire sample by combustion, the three similar values suggest that the -SO$_3$H groups are homogeneously distributed on the surface of GO-50, rather than only located at the edges of GO sheets [59]. This property will be beneficial to heterogeneous catalytic reactions as the reactants can get better contact with catalytic active sites on both sides of GO-50. The detailed atomic content, XPS survey, C 1s, S 2p XPS spectra of GO-50, S-GO-50, S-RGO, S-SWCNT, Glu-TSOH, GO-2 and GO-3 were also measured and the results are shown in Fig. S10.
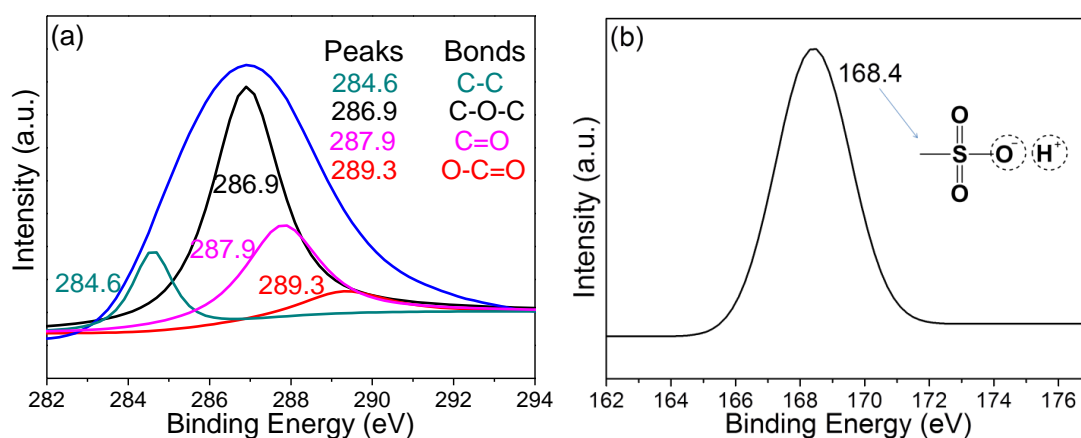

Fig.6 High resolution C 1s XPS spectra (a) and S 2p XPS spectra (b) of the GO-50

3.1.5 TGA-DSC of FGO samples

TGA-DSC was conducted under N_2 atmosphere to evaluate the thermal properties of graphite and FGO samples and the results are illustrated in Fig. 7. The weight loss is only observed at over 700 ℃ for graphite, suggesting that there are almost no functional groups in the raw graphite. Two major mass loss regions can be observed from the DSC curves of GO samples (Fig. 7b). The first weight loss peak centering 240 ℃ is aroused from the decomposition of oxygen-containing functional groups, such as -COOH and -SO_3H groups [50]. It is noteworthy that the weight losses in this stage are about 35, 40 and 50 wt. % for GO-50, GO-75 and GO-100, respectively, which is in fairly good agreement with the data from elemental analysis results in Table 2. The weight loss centering in 240 ℃ also reveals that the prepared GO samples would be potentially vital for reusing especially in medium-temperature (e.g. lower than 200 ℃) reactions like esterification. The second peak over 600 ℃ is ascribed to the decomposition of graphene framework [57].
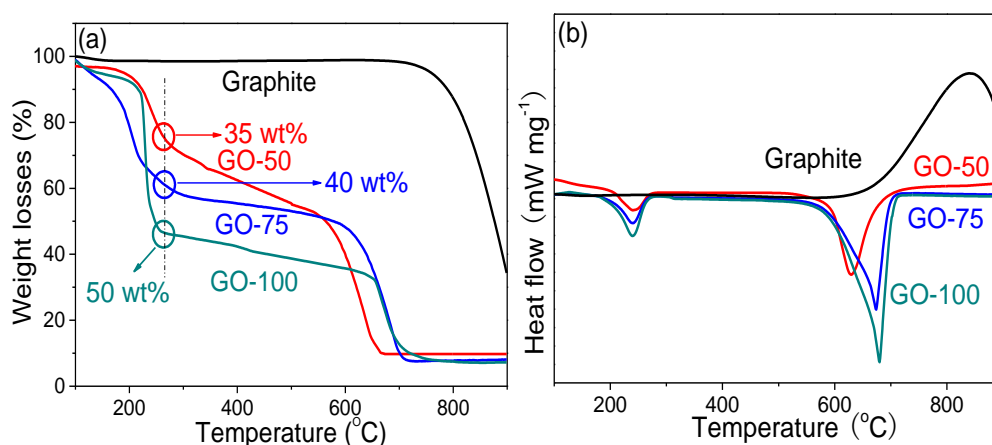

Fig.7 TGA (a) and DSC (b) diagrams of pristine graphite, GO-50, GO-75 and GO-100

3.2 Esterification by GO samples

3.2.1 The selection of acid amount for catalytic performance comparison

Esterification reactions were firstly carried out with different sulfuric acid amounts to establish the acid amount for catalytic performance comparison and the results are illustrated in Fig. S5. The oleate yield increases greatly from 78.4 to 90.7 % while the TOF value decreases 25 times when the H^+ amount increases from 0.25 mmol to 10 mmol. Therefore, the H^+ amount of 0.25 mmol was used in the

subsequent experiments.

3.2.2 Esterification catalyzed by various nanocarbon-based catalysts

All the prepared FGO samples with 0.25 mmol H^+ were used in esterification to evaluate their catalytic activity and the results are shown in Fig. 8 (a). The results of esterification catalyzed by acetic acid, H_2SO_4 and that without catalyst are also compared. The yield is about 4.2% when no catalyst was added in the reaction medium because oleic acid itself could act as a weak acid catalyst [60]. The yield by acetic acid could slightly promote the yield to 8.4 % since acetic acid is a stronger acid compared to oleic acid (Table 2). GO-2 and GO-3 exhibited poor catalytic activity because of the low catalytic active sites, the sulfonated groups (Table 2). It is also noteworthy in Fig. 8(a) that the catalytic activity of GO-50 is greatly larger than that of GOite-50 despite the same elemental compositions. This shows the importance of the unique open 2D structure of GO-50, which enables the excellent access of reactants to active sites on both sides of GO-50. All the three prepared FGO samples (GO-50, GO-75 and GO-100) showed excellent catalytic activity among all the catalysts under the same H^+ amount of 0.25 mmol. Specifically, GO-50 had the highest esterification conversion of over 92 % after 8 hours, which is much higher than the yield by sulfuric acid (78.4 %). This can be explained by the existence of weak acidic groups on the FGO sheets and the synergistic effect of $-SO_3H$ with $-COOH$ groups, which promote the esterification. This hypothesis was also confirmed by the fact that S-GO-50 performed less well compared with GO-50 and the yield is only 75.7 % after 8 h although S-GO-50 contains over twice amount of $-SO_3H$ groups (Table 2). As a control experiment, GO-50 was treated at 300 ℃ for 12 h to remove all the oxygen-containing functional groups and to produce TGO-50-300. The resulting sample showed very poor catalytic performance in esterification and the yield is only 7.8 % after 8 h. Additional supplementary experiments were performed using acetic acid as a model carboxylic group to verify the proposition that there is synergistic effect between $-SO_3H$ and $-COOH$ groups, and the results are shown in Fig. S6. The oleate yield of 8 h was only 6.4 % and 36.5 %, respectively, when 0.009 g acetic acid and 0.043 g S-GO-50 were used as separated catalysts. However, when 0.009 g acetic

acid and 0.043 g S-GO-50 were used together as a "co-catalyst", the oleate yield reached 74.5 %, which is much higher than the sum of the oleate yields (42.9 %) by the two single catalysts. It is also noteworthy that despite having the same amount of -COOH and -SO_3H, the yield by GO-50 is 18 % higher than that of the "co-catalyst". This might result from that the adsorption-desorption equilibrium on the surface of the carbon, which enriches oleic acid near the active sites and facilitates the esterification [51]. Since acetic acid has been widely used as a reactant with alcohols in esterification [27, 57, 61-64], the product distributions of esterification catalyzed by S-GO-50, acetic acid, the "co-catalyst" and GO-50 were studied and the results are illustrated in Table S 10. It is found that apart from methyl oleate, trace amount of methyl acetate was produced when acetic acid and the "co-catalyst" were used as catalyst, suggesting that acetic acid prefers to be an acid catalyst, rather than a reactant in this typical reaction system. This can be explained by the fact that acetic acid is a stronger acid compared to oleic acid as oleic acid displayed higher pH compared with acetic acid (Fig. S11).

The synergistic effect between -SO_3H and -COOH groups was also confirmed by using both homogeneous and heterogeneous systems. In the homogeneous catalytic esterification system, the oleate yield is 6.4 % and 78.4 % when acetic acid (0.009 g) and H_2SO_4 (0.25 mmol) was used as separate catalyst, respectively. However, when acetic acid and H_2SO_4 were used together as co-catalyst, the oleate yield reached 95.1 %, which is higher than the sum of the oleate yields (84.80 %) by the two single catalysts (Fig. S7a). In the heterogeneous catalytic esterification system, the yield is only 48.1 % when Amberlyst-15 (0.036 g) is used as catalyst. However, the yield of methyl oleate is 70.7 % when acetic acid (0.009 g) and Amberlyst-15 (0.036 g) were used as co-catalyst (Fig. S7b). All the results mentioned above confirmed the existence of the synergistic effect between -SO_3H and -COOH groups that enhanced the catalytic activity of GO-50.
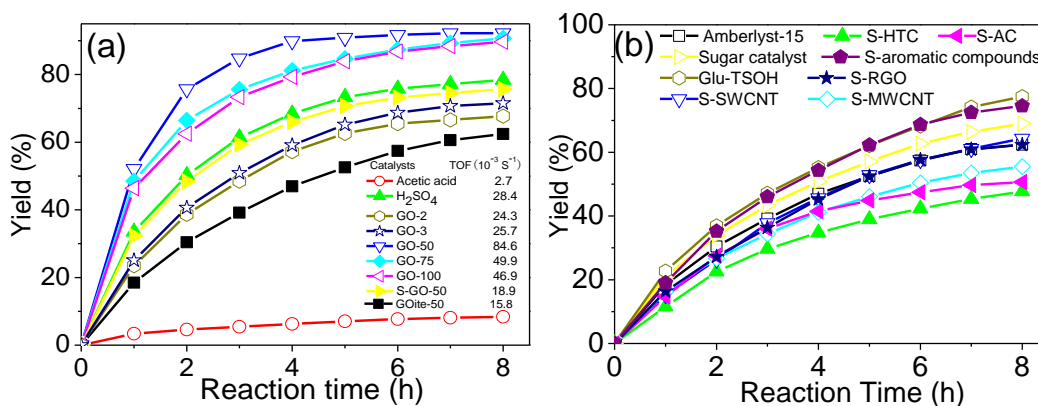
Fig.8 Esterification of oleic acid with methanol catalyzed by different catalysts (Graphene oxide materials (a); Amberlyst-15 and other carbon-based solid materials (b); Reaction conditions: oleic acid 20 g, methanol 50 g, catalyst loading 0.25 mmol H^+, temperature 338 K and mechanical stirring rate 360 rpm)

Eight typical previously reported carbon-based solid catalysts, including five kind of 3-D catalysts including sulfonated-activated carbon (S-AC), sulfonated-aromatic compounds, glucose-p-toluene sulfonic acid (Glu-TSOH), sulfonated-hydrothermal carbon (S-HTC), sugar catalyst; 2-D sulfonated-reduced graphene oxide (S-RGO); and two 1-D catalysts including sulfonated single-walled carbon nanotubes (S-SWCNT), sulfonated multiple-walled carbon nanotubes (S-MWCNT) were resynthesized strictly according to the literatures. The detailed chemical and textural characteristics of these catalysts were studied and illustrated in Table S3. To do safer comparisons, the catalytic activities of these resynthesized carbon-based catalysts were tested under their original reaction conditions respectively and the results are illustrated in Table S4. It is found that the catalytic activity of individual catalyst is almost the same with the original reported results despite a little deactivation. The catalytic activities of the prepared FGO samples were further compared with Amberlyst-15 and these typical carbon-based solid catalysts under this typical reaction conditions. Based on the results shown in the Fig.8 (b), the catalytic activity of GO-50 also surpasses that of all the nine solid acid catalysts.

3.2.3 The calculation of TOF values catalyzed by various catalysts

A comparison of the TOF values of esterification catalyzed by different catalysts calculated from reaction rate constants (shown in Fig. 9) is provided in Fig. 8 and

Table 3. The TOF values of Amberlyst-15 and sulfuric acid are 2.8×10^{-3} and 28.4×10^{-3} s^{-1}, respectively, due to the fact that sulfuric acid is homogeneous and therefore provides more accessible catalytic sites [51]. GO-50, GO-75 and GO-100 have higher TOF values than that of sulfuric acid because the latter has much higher $-SO_3H$ concentration but contains no -COOH group. Specifically, TOF value of esterification by GO-50 is 84.6×10^{-3} s^{-1}, which is 3 times higher than that of sulfuric acid, indicating that GO-50 has higher intrinsic catalytic activity and further suggesting the existence of synergistic effect of $-SO_3H$ with -COOH groups. It is clearly found that the order of the TOF numbers for all these carbon-based solid acids is 2-D > 1-D > 3-D materials, this is mainly because the layered 2-D structure maximizes the solid/liquid interface and minimizes the mass transfer resistance and thus favours the heterogeneous esterification reaction.

Table 3 TOF of various catalysts in esterification using the same amount of acid (H^+): 0.25 mmol (2-D materials in left column; 3-D, 1-D materials and Amberlyst-15 in the right column)

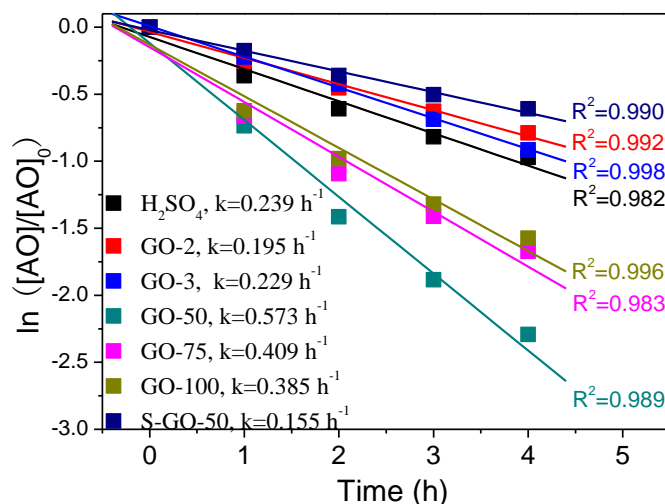| Samples	$-COOH/SO_3H$ molar ratio	TOF (10^{-3} s^{-1})	Samples	$-COOH/SO_3H$ molar ratio	TOF (10^{-3} s^{-1})
GO-50	1.8	84.6	S-AC	0.11	12.8
GO-75	2.1	49.9	S–aromatic compounds	0.11	14.1
GO-100	2.2	46.9	S–HTC	0.06	10.4
GO-2	0.16	24.3	Glu–TSOH	0.14	16.1
GO-3	0.18	25.7	Sugar catalyst	0.3	18.7
S-GO-50	0.15	18.9	S–SWCNT	0.4	20.1
S-GO-50 + Acetic acid	1.8	52.8	S–MWCNT	0.6	19.4
S–RGO	0.17	22.2	Amberlyst-15	—	2.8

Fig.9 Linear relationships between ln([AO]/[AO]$_0$) and reaction time t for esterification reactions catalyzed by various catalysts at 65 ℃ (AO: acidified oil)

The order of the TOF values is Sugar catalyst > Glu-TSOH > S-aromatic compounds > S-AC > S-HTC for all the catalysts with 3-D structure, which can be explained by the effect of -COOH/-SO$_3$H molar ratio. As shown in Fig. 10(a), the TOF value increases slightly when the -COOH/-SO$_3$H molar ratio increases from 0.06 (for S-HTC) to 0.3 (for Sugar catalyst), suggesting that there is an enhancement of -SO$_3$H acidity by combining with -COOH groups in catalyzing esterification. It is also noted that S-aromatic compounds possesses higher TOF value compared with S-AC although they have the same -COOH/-SO$_3$H molar ratio (0.11), which is mainly due to the much higher content of oxygen-containing functional groups in S-aromatic compounds. Similar phenomenon is also observed for the catalysts with 2-D structure (Fig. 10(b)). The TOF values increases dramatically from 18.9 to 84.6 $\times 10^{-3}$ s^{-1} when the -COOH/-SO$_3$H molar ratio increases from 0.15 (for S-GO-50) to 1.8 (for GO-50). However, the further increment of the -COOH/-SO$_3$H molar ratio leads to lower TOF values (for GO-75 and GO-100), which is probably because that the accessibility of the -SO$_3$H groups is reduced when the -COOH density is extraordinarily high. Additionally, the calculated TOF of the "co-catalyst" (S-GO-50 + Acetic acid), 52.8 $\times$ 10^{-3} s^{-1}, is much greater than that of S-GO-50 (18.9 $\times 10^{-3}$ s^{-1}), further confirming the effect of -COOH groups on promoting esterification catalytic reactivity. It is also noteworthy that despite having the same amount of -COOH and -SO$_3$H, the TOF of

GO-50 is 1.6 times higher than that of the "co-catalyst". This might result from the enrichment of oleic acid and methanol molecules near the $-SO_3H$ groups on the graphene sheets in GO-50 through adsorption and hydrogen bonding, which facilitates the reaction. For the catalysts with 1-D structure, S-SWCNT possesses almost the same TOF value with that of S-MWCNT although the latter has higher $-COOH/-SO_3H$ molar ratio. This is probably because the affinity of S-SWCNT to the reactants is much better than that of S-MWCNT arousing from its single-walled structure and higher exposure of active sites [65]. Based on all the discussions above, the prominent catalytic performance of GO-50 can be attributed to its three unique features, i.e., the layered 2-D structure, the enrichment of oxygen-containing functional groups and the desirable $-COOH/-SO_3H$ molar ratio.
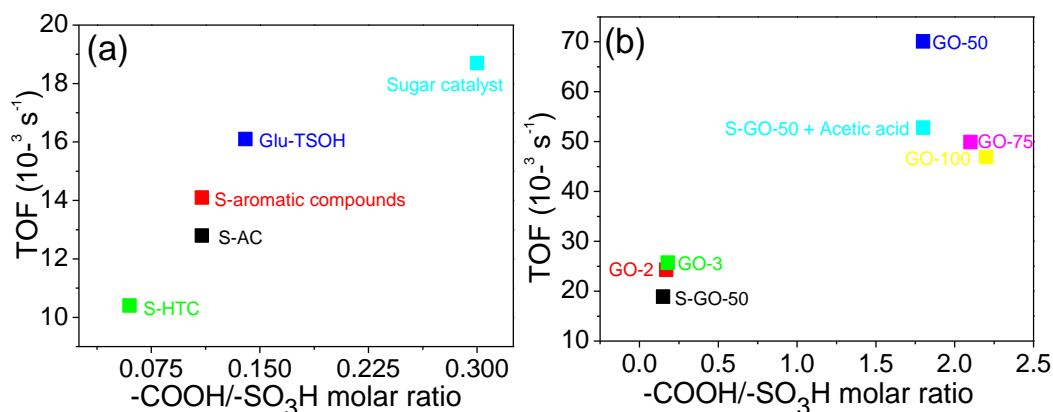

Fig.10 The relationship between $-COOH/-SO_3H$ molar ratio in catalysts and its corresponding TOF value for 3-D (a) and 2-D (b) materials

3.2.4 Reaction kinetics

As shown in Fig. 11, the plot of $\ln k$ versus $1/T$ can be represented by a straight line and the apparent activation energy (E_a) of esterification by S-GO-50 is determined to be 41.9 kJ mol^{-1}. E_a decreases to 34.3 kJ mol^{-1} for the "co-catalyst", suggesting the improvement of "acidity" of $-SO_3H$ groups by the combination with $-COOH$ groups in the catalysis esterification. The apparent activation energy esterification by GO-50 is 25.7 kJ mol^{-1}, lower than the value of the "co-catalyst". This might result from that the adsorption-desorption equilibrium on the surface of the carbon, which enriches oleic acid near the active sites on the graphene sheets in GO-50 and facilitates the esterification [51].
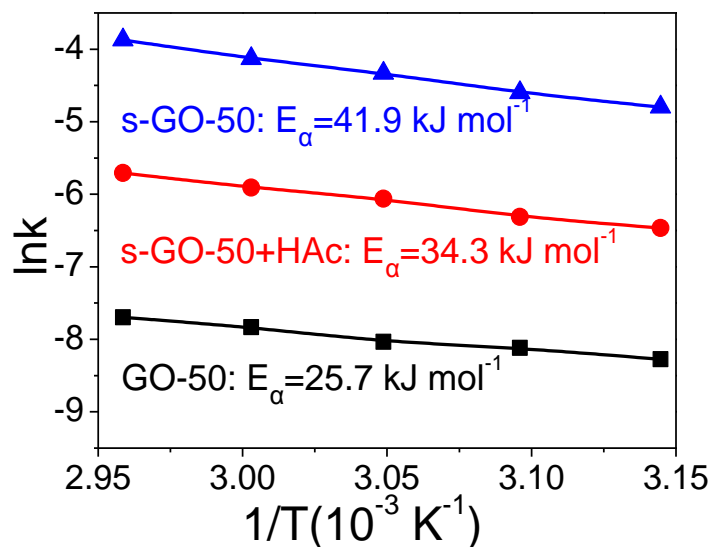
Fig.11 The linear Arrhenius equation fitted between ln$k$ and 1/T to obtain the apparent

activation energy

3.2.5 Esterification process catalyzed by GO-50

The esterification process of oleic acid with methanol catalyzed by GO-50 experienced three main steps (Fig. 12): 1) diffusion of oleic acid and methanol into the GO-50 layers and this step processed fairly fast due to the fact that the molecular diameters of oleic acid (0.5 nm) and methanol (0.43) are lower than the interlayer spacing of GO-50 (0.72 nm); 2) chemical absorption and surface reaction on the GO-50; 3) diffusion of the produced methyl oleate and water out of catalysts layers to surface and liquid phase.
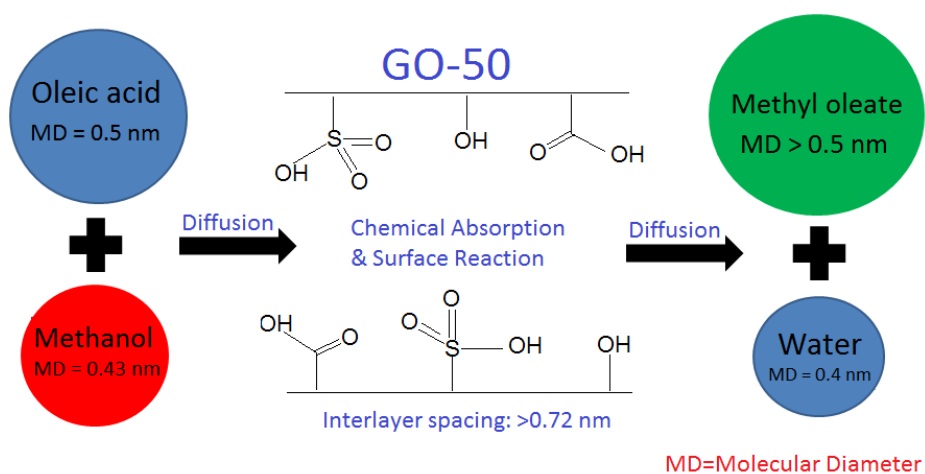

Fig.12 The total esterification process catalyzed by GO-50

The esterification mechanism of oleic acid with methanol catalyzed by strong acid catalysts containing -SO₃H groups has been intensively studied [6, 66, 67] and is illustrated in Fig. S8. The catalytic esterification occurs in the following steps: 1) the protonation at the carbonyl oxygen of oleic acid and the generation of carbocation (A); 2) the nucleophilic attack at the positive carbon atoms by the hydroxyl group in methanol and the generation of an unstable intermediate (B); 3) the removal of proton from the unstable intermediate (B) and the production of methyl oleate and water. In this well-established esterification mechanism, methanol does not engage in the esterification until the second step because -SO₃H is a strong acidic group while methanol is a weak alkali in the view of the Lewis acid-base theory. Therefore, the strong acidic nature of -SO₃H makes it difficult to protonate the methanol molecule. However, when the weak acid group such as -COOH is added, the deprotonated form of -COOH could generate hydrogen bond with -OH group in the methanol molecule, providing a small portion of "negative charge" to the oxygen in methanol molecule. This "negative charge" in turn promotes the nucleophilicity of methanol molecule and hences the esterification reaction rate and conversion. The detailed esterification mechanism catalyzed by GO-50 is proposed based on the well-documented mechanism and all the discussions mentioned above. As illustrated in Fig. 13, the esterification mainly contains 5 reaction paths which are deliberately divided into 3 steps. In the first step, two reaction processes occur simultaneously: 1) the protonation of carbonyl group in oleic acid and the generation of carbocation (A) and 2) the deprotonation of -COOH groups and the formation of hydrogen bond with methanol (B). nucleophilic attack of negative charge with both methanol (1) and "methanol with negative charge"(2) form the unstable intermediate (C) in the second step. In the third step, the proton is removed from the unstable intermediate (C) and then methyl oleate and water are produced; simultaneously, the catalyst is regenerated to start another catalytic cycle.
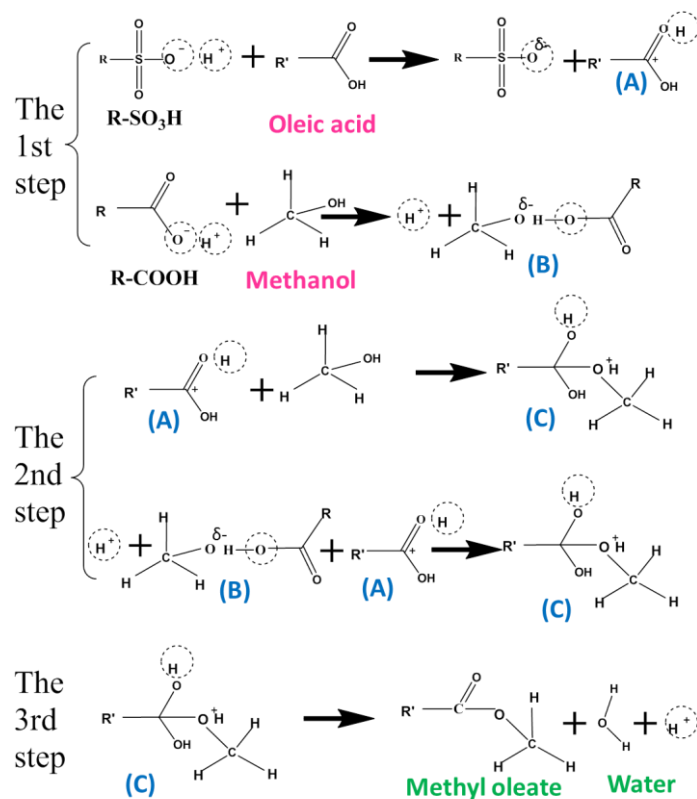
Fig.13 Proposed esterification mechanism catalyzed by GO-50 (The reactants are labelled in magenta, the intermediates are labelled in blue and the products are labelled in green)

3.2.6 Reusability

Besides catalytic activity, the reusability of catalyst is key to curtailing production cost. The catalytic stability of GO-50 was evaluated by running esterification for four times and the results of GO-2, GO-3 and S-GO-50 were used as control, respectively. As shown in Table 4, although all the four catalysts showed a slight decline in yield after one cycle of reuse, GO-50 shows superior reusability compared to the other three GO catalysts and the oleate yield of 8 h decreases slightly from 92.2 % to 87.5 % after 3 runs. However, much more significant deactivation and distinct drops in catalytic activity are observed for GO-2, GO-3 and S-GO-50. The remarkable reusability of GO-50 is also attributed to the higher -COOH/-SO₃H molar ratio of GO-50 (1.8) than the other three GO samples (0.16, 0.18, and 0.15 mmol g⁻¹ for GO-2, GO-3 and S-GO-50, respectively).

Table 4 Oleate yield of 8 h for all the FGO samples with the same amount of acid (H^+): 0.25 mmol

Catalysts	Run 1 (%)	Run 2 (%)	Run 3 (%)	Run 4 (%)
GO-50	92.2	90.5	89.6	87.5
GO-2	67.7	64.5	61.2	50.6
GO-3	71.5	68.5	62.5	52.2
S-GO-50	75.7	71.4	67.7	65.4

Generally speaking, carbon-based solid acid catalysts normally lose their catalytic activities due to the leaching of sulfonated groups in aqueous suspensions, especially in water participating reactions such as esterification and hydrolysis [45, 68]. To investigate the slight deactivation of GO-50, the sulfur content in GO-50 and in the reaction suspension before and after each esterification run were studied and no leaching of S from GO-50 was observed even after 4 runs (Table 5). Both of the two results suggest that the slight deactivation of GO-50 is not because of the hydrolysis of -SO_3H groups, but -SO_3H groups being blocked by the byproducts [45, 50].

Table 5 Sulfur content in GO-50 and reaction solution after each reaction cycle

Run	Sulfur content in GO-50 (wt. %) [a]	Sulfur content in the reaction solution (ppm) [b]
1	2.89	21.3
2	2.87	21.3
3	2.85	21.3
4	2.85	21.4

[a] obtained by elemental analysis; [b] determined by micro-coulometry analysis.

3.3 Esterification by GO-50/PES catalytic membranes

Based on the above findings, GO-50 is a cost-effective and highly-efficient catalyst for esterification reaction. However, GO-50 still needs to be separated from the reaction mixtures and undertaken post-treatment before the reutilization. Therefore, a GO-50/PES catalytic membrane, which can be used directly in membrane reactor, was prepared and used as solid acidic catalyst for esterification.

3.3.1 Appearance of the prepared GO-50/PES membrane

Fig. 14 shows the digital photographs of GO-50/PES catalytic membrane (mass ratio 1: 20, annealed at 200 ℃) with the thickness of 0.2 mm and 0.5 mm, respectively. This membrane is a smooth, uniform and black paper-like material with high elasticity. The membrane also displays high heating resistance, which can maintain its structure at high temperature of 200 ℃.
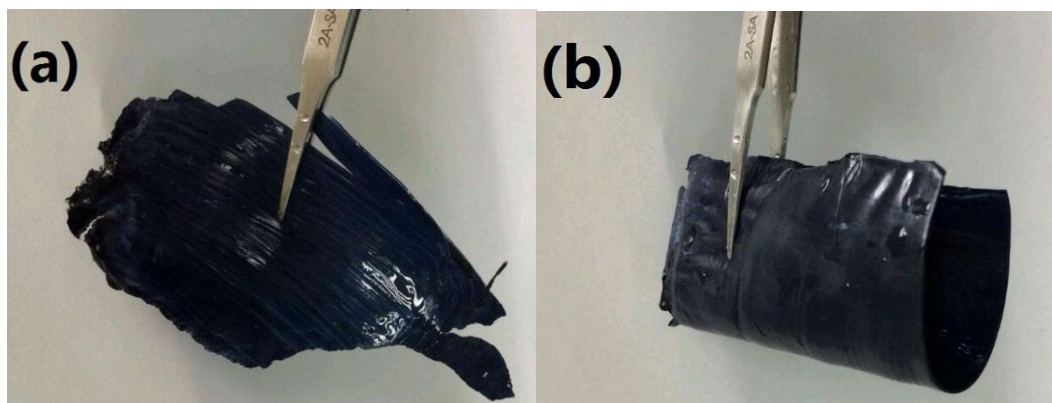

Fig.14 Appearances of GO-50/PES catalytic membrane annealed at 200 ℃ with the thickness of 0.2 mm (a) and 0.5 mm (b)

3.3.2 Catalytic activity of the GO-50/PES catalytic membrane

Effect of GO-50/PES mass ratio, membrane annealing temperature, membrane thickness, membrane quantity, reaction temperature, and methanol/oleic acid mass ratio on esterification conversion were systematically studied and the results are shown in Fig. S9. The optimal reaction conditions are: GO-50: PES mass ratio of 1: 5, membrane annealing temperature of 150 ℃, membranes thickness of 0.1 mm, membrane loading of 4 g, reaction temperature of 65 ℃, methanol/oleic acid mass ratio of 2: 1. The esterification was performed under optimal reaction conditions and the results are shown in Fig. 15. As can be seen in Fig. 15, the yield of methyl oleate is about 94 % after 8 h, suggesting that esterification catalyzed by GO-50/PES catalytic membrane is an appropriate option for biodiesel production since it is an economical and easy route. The GO-50/PES also showed excellent catalytic stability with only 8 % deactivation even after 6 runs (yield of 85.6 %). In the future work, the GO-50/PES catalytic membrane will be used in a home-made catalytic membrane reactor to evaluate the catalytic stability in continuous esterification reaction.
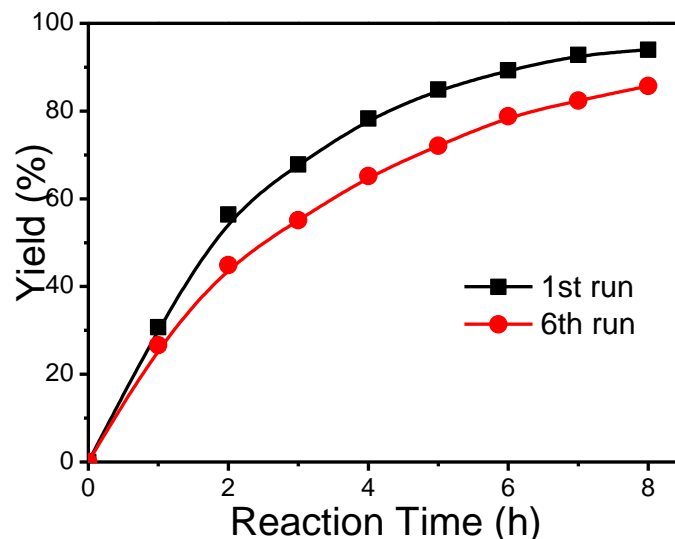
Fig.15 Esterification catalyzed by GO-50/PES membrane under optimal conditions

4. Conclusion

Functional graphene oxide (FGO) samples have been prepared readily with a simple modified Hummers' method and found to be highly active and reusable carbon-based solid acid catalysts for the esterification of oleic acid with methanol to produce biodiesel. It is found that the order of the TOF value is 2-D > 1-D > 3-D materials for all the carbon-based solid acids. Furthermore, the -COOH/-SO$_3$H molar ratio played significant roles in esterification for the carbon-based solid acid catalysts with the same dimensionality. Specifically, both catalysts with low (i. e. 0.06) and much too high (i. e. 2.1) -COOH/-SO$_3$H molar ratio have lower TOF, suggesting an enhancement of -SO$_3$H acidity by the combination with desirable -COOH density. Among all the catalysts studied, GO-50 bearing -SO$_3$H and -COOH groups have exhibited remarkable catalytic performance in esterification and higher TOF value compared with the other carbon-based solid acid catalysts and sulfuric acid. The reaction kinetics and mechanism of the esterification by GO-50 have been investigated in detail. In addition, GO-50/PES composite membrane has been prepared and employed successfully in esterification and the optimal reaction conditions have been comprehensively studied. The GO-50/PES catalytic membrane showed promising potential in the large scale and continuous production of biodiesel.

Acknowledgements

Reference

[1] Ma F, Hanna MA. Biodiesel production: a review. Bioresour Technol. 1999;70(1):1-15.

[2] Liu R, Wang X, Zhao X, Feng P. Sulfonated ordered mesoporous carbon for catalytic preparation of biodiesel. Carbon. 2008;46(13):1664-9.

[3] Avhad MR, Marchetti JM. Innovation in solid heterogeneous catalysis for the generation of economically viable and ecofriendly biodiesel: A review. Catalysis Reviews. 2016:1-52.

[4] Talebian Kiakalaieh A, Amin NAS, Mazaheri H. A review on novel processes of biodiesel production from waste cooking oil. Appl Energy 2013;104:683-710.

[5] Farooq M, Ramli A, Naeem A. Biodiesel production from low FFA waste cooking oil using heterogeneous catalyst derived from chicken bones. Renewable Energy 2015;76:362-8.

[6] Zhang H, Gao J, Zhao Z, Chen GZ, Wu T, He F. Esterification of fatty acids from waste cooking oil to biodiesel over a sulfonated resin/PVA composite. Catal Sci Tech. 2016;6(14):5590-8.

[7] Marchetti J, Errazu A. Esterification of free fatty acids using sulfuric acid as catalyst in the presence of triglycerides. Biomass Bioenerg. 2008;32(9):892-5.

[8] DeSimone JM. Practical Approaches to Green Solvents. Science. 2002;292:799-803

[9] Hara M, Yoshida T, Takagaki A, Takata T, Kondo JN, Hayashi S, et al. A carbon material as a strong protonic acid. Angew Chem Int Ed. 2004;43(22):2955-8.

[10]Boz N, Degirmenbasi N, Kalyon DM. Esterification and transesterification of waste cooking oil over Amberlyst 15 and modified Amberlyst 15 catalysts. Appl Catal, B-Environ. 2015;165:723-30.

[11]Saravanan K, Tyagi B, Shukla RS, Bajaj HC. Esterification of palmitic acid with methanol over template-assisted mesoporous sulfated zirconia solid acid catalyst. Appl Catal, B-Environ. 2015;172-173:108-15.

[12]Saravanan K, Tyagi B, Bajaj HC. Nano-crystalline, mesoporous aerogel sulfated zirconia as an efficient catalyst for esterification of stearic acid with methanol. Appl Catal, B-Environ. 2016;192:161-70.

[13]Guo Q, Fan F, Pidko EA, van der Graaff WNP, Feng Z, Li C, et al. Highly Active and Recyclable Sn-MWW Zeolite Catalyst for Sugar Conversion to Methyl Lactate and Lactic Acid. ChemSusChem. 2013;6(8):1352-6.

[14]Casimiro MH, Silva AG, Alvarez R, Ferreira LM, Ramos AM, Vital J. PVA supported catalytic membranes obtained by γ-irradiation for biodiesel production. Radiat Phys Chem 2014;94:171-5.

[15]Zhang H, Ding J, Qiu Y, Zhao Z. Kinetics of esterification of acidified oil with different alcohols by a cation ion-exchange resin/polyethersulfone hybrid catalytic membrane. Bioresour Technol. 2012;112:28-33.

[16]Hara M. Biomass conversion by a solid acid catalyst. Energy Environ Sci. 2010;3(5):601-7.

[17]Suganuma S, Nakajima K, Kitano M, Hayashi S, Hara M. sp(3) -linked amorphous carbon with sulfonic acid groups as a heterogeneous acid catalyst. ChemSusChem. 2012;5(9):1841-6.

[18]Malins K, Kampars V, Brinks J, Neibolte I, Murnieks R. Synthesis of activated carbon based heterogenous acid catalyst for biodiesel preparation. Appl Catal, B-Environ. 2015;176-177:553-8.

[19]Liang X, Zeng M, Qi C. One-step synthesis of carbon functionalized with sulfonic acid groups using hydrothermal carbonization. Carbon. 2010;48(6):1844-8.

[20]Shuit SH, Tan SH. Feasibility study of various sulphonation methods for transforming carbon nanotubes into catalysts for the esterification of palm fatty acid distillate. Energy Convers Manage 2014;88:1283-9.

[21]Toda M, Takagaki A, Okamura M, Kondo JN, Hayashi S, Domen K, et al. Biodiesel made with sugar catalyst. Nature. 2005;438:10.

[22]Antunes MM, Russo PA, Wiper PV, Veiga JM, Pillinger M, Mafra L, et al. Sulfonated graphene oxide as effective catalyst for conversion of 5-(hydroxymethyl)-2-furfural into biofuels. ChemSusChem. 2014;7(3):804-12.

[23]Wang J, Xu W, Ren J, Liu X, Lu G, Wang Y. Efficient catalytic conversion of fructose into hydroxymethylfurfural by a novel carbon-based solid acid. Green Chem. 2011;13(10):2678.

[24]Hu L, Lin L, Wu Z, Zhou S, Liu S. Chemocatalytic hydrolysis of cellulose into glucose over solid acid catalysts. Appl Catal, B-Environ. 2015;174-175:225-43.

[25]Tao H, Yan C, Robertson AW, Gao Y, Ding J, Zhang Y, et al. N-Doping of graphene oxide at low temperature for the oxygen reduction reaction. Chem Commun. 2017;53(5):873-6.

[26]Sun Z, Masa J, Weide P, Fairclough SM, Robertson AW, Ebbinghaus P, et al. High-quality functionalized few-layer graphene: facile fabrication and doping with nitrogen as a metal-free catalyst for the oxygen reduction reaction. J Mater Chem A. 2015;3(30):15444-50.

[27]Nakajima K, Hara M. Amorphous Carbon with SO3H Groups as a Solid Brønsted Acid Catalyst. ACS Catal. 2012;2(7):1296-304.

[28]Poonjarernsilp C, Sano N, Tamon H. Hydrothermally sulfonated single-walled carbon nanohorns for use as solid catalysts in biodiesel production by esterification of palmitic acid. Appl Catal, B-Environ. 2014;147:726-32.

[29]Xu Y, Hong W, Bai H, Li C, Shi G. Strong and ductile poly(vinyl alcohol)/graphene oxide composite films with a layered structure. Carbon. 2009;47(15):3538-43.

[30]Chen Y, Zhang X, Zhang D, Yu P, Ma Y. High performance supercapacitors based on reduced graphene oxide in aqueous and ionic liquid electrolytes. Carbon. 2011;49(2):573-80.

[31] Amiinu IS, Zhang J, Kou Z, Liu X, Asare OK, Zhou H, et al. Self-Organized 3D Porous Graphene Dual-Doped with Biomass-Sponsored Nitrogen and Sulfur for Oxygen Reduction and Evolution. ACS Applied Materials & Interfaces. 2016;8(43):29408-18.

[32] He D, Xiong Y, Yang J, Chen X, Deng Z, Pan M, et al. Nanocarbon-intercalated and Fe–N-codoped graphene as a highly active noble-metal-free bifunctional electrocatalyst for oxygen reduction and evolution J Mater Chem A. 2017;5:1930-4

[33] Liu X, Amiinu IS, Liu S, Pu Z, Li W, Ye B, et al. H2O2-Assisted Synthesis of Porous N-Doped Graphene/Molybdenum Nitride Composites with Boosted Oxygen Reduction Reaction. Advanced Materials Interfaces. 2017;4(11):1601227.

[34] Novoselov KS, Geim AK, Morozov SV, Jiang D, Zhang Y, Dubonos SV, et al. Electric Field Effect in Atomically Thin Carbon Films. Science. 2004;306(5096):666-9.

[35] Stankovich S, Dikin DA, Piner RD, Kohlhaas KA, Kleinhammes A, Jia Y, et al. Synthesis of graphene-based nanosheets via chemical reduction of exfoliated graphite oxide. Carbon. 2007;45(7):1558-65.

[36] He D, Kou Z, Xiong Y, Cheng K, Chen X, Pan M, et al. Simultaneous sulfonation and reduction of graphene oxide as highly efficient supports for metal nanocatalysts. Carbon. 2014;66:312-9.

[37] Daniela CM, Dmitry VK, Jacob M. Berlin, Alexander Sinitskii, Zhengzong Sun, Alexander Slesarev, et al. Improved synthesis of graphene oxide. ACSnano. 2010;4(8):4806-14.

[38] Kim J, Cote LJ, Kim F, Yuan W, Shull KR, Huang J. Graphene Oxide Sheets at Interfaces. J Am Chem Soc. 2014;132:8180-6.

[39] Anton Lerf, Heyong He, Michael Forster, Klinowski J. Structure of Graphite Oxide Revisited. J Phys Chem B. 1998;102(23):4477-82.

[40] Zhao X, Wang J, Chen C, Huang Y, Wang A, Zhang T. Graphene oxide for cellulose hydrolysis: how it works as a highly active catalyst? Chem Commun. 2014;50(26):3439-42.

[41] Primo A, Puche M, Pavel OD, Cojocaru B, Tirsoaga A, Parvulescu V, et al. Graphene oxide as a metal-free catalyst for oxidation of primary amines to nitriles by hypochlorite. Chem Commun. 2016;52(9):1839-42.

[42] Zhu S, Chen C, Xue Y, Wu J, Wang J, Fan W. Graphene Oxide: An Efficient Acid Catalyst for Alcoholysis and Esterification Reactions. ChemCatChem. 2014;6(11):3080-3.

[43] Hummers WS, Offeman RE. Preparation of Graphitic Oxide. J Am Chem Soc. 1958;80(6):1339.

[44] Foo GS, Sievers C. Synergistic effect between defect sites and functional groups on the hydrolysis of cellulose over activated carbon. ChemSusChem. 2015;8(3):534-43.

[45] Van Pelt AH, Simakova OA, Schimming SM, Ewbank JL, Foo GS, Pidko EA, et al. Stability of functionalized activated carbon in hot liquid water. Carbon. 2014;77:143-54.

[46] Gupta VK, Atar N, Yola ML, Ustundag Z, Uzun L. A novel magnetic Fe@Au

core-shell nanoparticles anchored graphene oxide recyclable nanocatalyst for the reduction of nitrophenol compounds. Water Res 2014;48:210-7.

[47]Stankovich S, Dikin D, Dommett HBG, Kohlhaas MK, Zimney JE, Stach AE, et al. Graphene-based composite materials. Nature. 2006;442(7100):282-6.

[48]Jeon I-Y, Shin Y-R, Sohn G-J, Choi H-J, Bae S-Y, Mahmood J, et al. Edge-carboxylated graphene nanosheets via ball milling. P Natl Acad Sci USA. 2012;109(15):5588-93.

[49]Shi P, Su R, Wan F, Zhu M, Li D, Xu S. Co3O4 nanocrystals on graphene oxide as a synergistic catalyst for degradation of Orange II in water by advanced oxidation technology based on sulfate radicals. Appl Catal, B-Environ. 2012;123-124:265-72.

[50]Zhang H, Luo X, Shi K, Wu T, He F, Zhou S, et al. Highly Efficient Sulfonic/Carboxylic Dual-Acid Synergistic Catalysis for Esterification Enabled by Sulfur-Rich Graphene Oxide. ChemSusChem. 2017;10:3352-7.

[51]Macia-Agull JA, Sevilla M, Maria A. Diez, Fuertes AB. Synthesis of Carbon-based Solid Acid Microspheres and Their Application to the Production of Biodiesel. ChemSusChem. 2010;3:1352-4.

[52]Bai J, Sun H, Yin X, Yin X, Wang S, Creamer AE, et al. Oxygen-Content-Controllable Graphene Oxide from Electron-Beam-Irradiated Graphite: Synthesis, Characterization, and Removal of Aqueous Lead [Pb(II)]. ACS Appl Mat Inter. 2016;8(38):25289-96.

[53]Biniak S, Szymański G, Siedlewski J, Świtkowski A. The characterization of activated carbons with oxygen and nitrogen surface groups. Carbon. 1997;35(12):1799-810.

[54]Paredes JI, Villar-Rodil S, Martı́nez-Alonso A, Tasco ń JMD. Graphene Oxide Dispersions in Organic Solvents. Langmuir. 2008;24(19):10560-4.

[55]Li D, Muller MB, Gilje S, Kaner RB, Wallace GG. Processable aqueous dispersions of graphene nanosheets. Nat Nanotechnol 2008;3(2):101-5.

[56]Pei S, Cheng H-M. The reduction of graphene oxide. Carbon. 2012;50(9):3210-28.

[57]Liu F, Sun J, Zhu L, Meng X, Qi C, Xiao F-S. Sulfated graphene as an efficient solid catalyst for acid-catalyzed liquid reactions. J Mater Chem. 2012;22(12):5495-502.

[58]Xing T, Li LH, Hou L, Hu X, Zhou S, Peter R, et al. Disorder in ball-milled graphite revealed by Raman spectroscopy. Carbon. 2013;57:515-9.

[59]Wang H, Deng T, Wang Y, Cui X, Qi Y, Mu X, et al. Graphene oxide as a facile acid catalyst for the one-pot conversion of carbohydrates into 5-ethoxymethylfurfural. Green Chem. 2013;15(9):2379-83.

[60]Liu Y, Lotero E, James G. Goodwin J. A comparison of the esterification of acetic acid with methanol using heterogeneous versus homogeneous acid catalysis. J Catal. 2006;242(2):278-86.

[61]Johnson RL, Anderson JM, Shanks BH, Schmidt-Rohr K. Simple One-Step Synthesis of Aromatic-Rich Materials with High Concentrations of Hydrothermally Stable Catalytic Sites, Validated by NMR. Chem Mater. 2014;26(19):5523-32.

[62]Jia R, Ren J, Liu X, Lu G, Wang Y. Design and synthesis of sulfonated carbons

with amphiphilic properties. J Mater Chem A. 2014;2(29):11195-201.

[63] Nabae Y, Liang J, Huang X, Hayakawa T, Kakimoto M-a. Sulfonic acid functionalized hyperbranched poly(ether sulfone) as a solid acid catalyst. Green Chem. 2014;16(7):3596-602.

[64] Ogino I, Suzuki Y, Mukai SR. Tuning the Pore Structure and Surface Properties of Carbon-Based Acid Catalysts for Liquid-Phase Reactions. ACS Catal. 2015;5(8):4951-8.

[65] Yu H, Jin Y, Li Z, Peng F, Wang H. Synthesis and characterization of sulfonated single-walled carbon nanotubes and their performance as solid acid catalyst. J Solid State Chem. 2008;181(3):432-8.

[66] Li J, Fu YJ, Qu XJ, Wang W, Luo M, Zhao CJ, et al. Biodiesel production from yellow horn (Xanthoceras sorbifolia Bunge.) seed oil using ion exchange resin as heterogeneous catalyst. Bioresour Technol. 2012;108:112-8.

[67] Tesser R, Casale L, Verde D, Di Serio M, Santacesaria E. Kinetics and modeling of fatty acids esterification on acid exchange resins. Chem Eng J 2010;157(2-3):539-50.

[68] Mo X, López DE, Suwannakarn K, Liu Y, Lotero E, James G. Goodwin J, et al. Activation and deactivation characteristics of sulfonated carbon catalysts. J Catal. 2008;254(2):332-8.